Spatio-Spectral Exploration Combining In Situ and Remote Measurements

David R. Thompson
Jet Propulsion Laboratory
California Institute of Technology
4800 Oak Grove Dr.
Pasadena, CA 91109
david.r.thompson@jpl.nasa.gov

David Wettergreen and **Greydon Foil**
The Robotics Institute
Carnegie Mellon University
5000 Forbes Ave.
Pittsburgh, PA 15213
{dsw,gfoil}@ri.cmu.edu

Michael Furlong
Intelligent Robotics Group
NASA Ames Research Center
Naval Air Station, Moffett Field
Mountain View, CA 94035
furlong@gmail.com

Anatha Ravi Kiran
Jet Propulsion Laboratory
California Institute of Technology
4800 Oak Grove Dr.
Pasadena, CA 91109
ravi.kiran@jpl.nasa.gov

Abstract

Adaptive exploration uses active learning principles to improve the efficiency of autonomous robotic surveys. This work considers an important and understudied aspect of autonomous exploration: *in situ* validation of remote sensing measurements. We focus on high-dimensional sensor data with a specific case study of spectroscopic mapping. A field robot refines an orbital image by measuring the surface at many wavelengths. We introduce a new objective function based on spectral unmixing that seeks pure spectral signatures to accurately model diluted remote signals. This objective reflects physical properties of the multi-wavelength data. The rover visits locations that jointly improve its model of the environment while satisfying time and energy constraints. We simulate exploration using alternative planning approaches, and show proof of concept results with the canonical spectroscopic map of a mining district in Cuprite, Nevada.

Introduction

A growing body of AI research tries to make robots more effective partners during remote exploration and survey. As rover traverse distance increases, it becomes increasingly important to incorporate science data into rover navigational and science activity planning (Thompson, Wettergreen, and Peralta 2011). Formalizing this process can enable rover autonomy that improves data collection during the long periods when the rover is out of touch with ground control (Wettergreen et al. 2008). By incorporating remote sensing into the automated science assessment, autonomous explorers can be more resilient to disruptions or opportunities, acting as a more informed proxy for the remote science team. Typical approaches involve detection and measurement of discrete features of interest (Estlin et al. 2006;

Wagstaff et al. 2013) or informative path and observation planning based on active learning or spatial experimental design (Thompson, Wettergreen, and Peralta 2011).

This work broadens adaptive exploration in two important directions. Most prior approaches to informative observation planning assume measurements at each location are scalar or uncorrelated with each other (e.g. Low, Dolan, and Khosla 2008 for a typical example). Here we address high-dimensional spectrometer data having strong correlations across dimensions. We also account for previous measurements of the explored area at different spatial and/or wavelength resolutions. This is important because, literalism aside, robotic space exploration seldom takes place in a vacuum; preparatory remote sensing almost always precedes the *in situ* traverse. These remote data inform, and largely prescribe, the exploration objectives. Such partnerships play to the strengths of both platforms: orbital measurements can identify investigation sites, and in situ sensors can provide more unambiguous interpretations.

We focus on the case of Visible to Shortwave Infrared (VSWIR) spectroscopy (Green et al. 1998; Plaza et al. 2009). In our scenario, a field robot refines a low-resolution orbital image using an in situ VSWIR reflectance spectrometer. VSWIR spectroscopy is a useful test case because of its ubiquity in terrestrial and planetary exploration. It contributes greatly to our understanding of mineralogy, atmospheric composition, and on Earth, agriculture, commerce, and the biosphere. However, orbital sensors have large pixel sizes (often 30m or more) so small localized features can go undetected. *In situ* sensing can complement these data by revealing pure signals from subpixel features. In-situ sensors also provide improved spectral resolution and signal to noise ratios (SNRs) which make them helpful for validating bulk properties of larger targets.

The paper defines a novel *spatio-spectral* exploration objective. Here the robot accumulates a spectral library that

facilitates *spectral unmixing* of the remote image. In other words, the it collects spectra that best explain the orbital measurements, seeking signatures that could physically reconstruct the spectra seen from orbit. This balances the competing objectives of sample diversity and representativeness, providing an unambiguous interpretation of the orbital data. A path planner visits features to optimize this objective while respecting a total budget on path cost. Regular replanning means the agent can recover from bad data (by adding additional spectra to the plan) and exploit new signals (by skipping future targets made redundant). We shall see that the objective is amenable to efficient path planning algorithms. The following sections give theoretical foundations for spatio-spectral exploration and then demonstrate different algorithm variants in simulation. In this demonstration the agent recomputes its course on the fly, adapting its path to visit distinctive spectral features that have not yet appeared in *in situ* data collection.

Background

Robotic Mapping for Exploration

There is a large body of previous work on robotic environmental sensing. Most formulations try to reconstruct the spatial structure of just one or two dependent variables of interest. This leads naturally to spatial statistical models like Gaussian Processes, reducing exploration to the well-understood problem of experimental design or active learning for regression. One typically optimizes information gain by maximizing the Shannon entropy of future observations, or by maximizing the Mutual Information with respect to unobserved locations (Cao, Low, and Dolan 2013). For example, Low et al. demonstrate information-theoretic loss functions that drive team of robots to reduce map uncertainty (Low, Dolan, and Khosla 2008). Diverse applications include measuring water constituents (Binney, Krause, and Sukhatme 2010) or current fields (Hollinger et al. 2012).

Recent research has started using remote sensing to guide robotic exploration. One study has demonstrated autonomous rover mapping based on an information gain objective, with a Gaussian Process model combining remote and *in situ* data about terrain properties (Thompson, Wettergreen, and Peralta 2011). There is also significant work to combine remote and in situ observations for hazard avoidance. These efforts typically involve Digital Elevation Models or visible-wavelength remote sensing channels (Silver, Bagnell, and Stentz 2010; Bagnell et al. 2010; Persson, Duckett, and Lilienthal 2008). They define or learn relationships between ground and remote data to improve navigation planning (Sofman et al. 2006). For example, Silver et al. (2010) demonstrate a self-training system where local observations train a classifier that predicts navigability throughout the orbital image. While this can be useful for path planning, it is not obvious how this approach could be extended to science-driven exploration or experimental design objectives.

The principles underlying the current work differ somewhat from these previous studies. To our knowledge ours is the first attempt to guide robotic exploration using full mul-
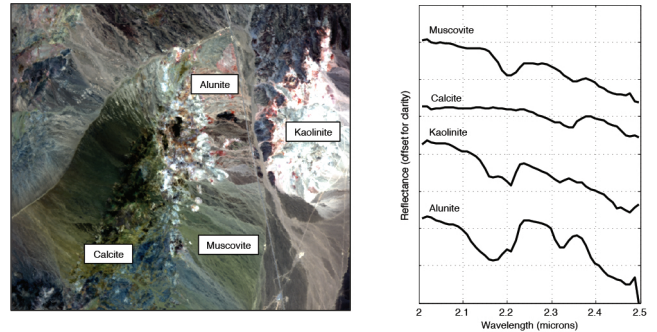

Figure 1: Spectral endmembers and characteristic absorption features

tivariate spectral data, and the powerful compositional information it provides. Here, we incorporate physical models of spectral mixing directly into the exploration objective. The resulting in situ measurements refine the remote signals, providing a combined measurement with the spectral precision of the former and the wide spatial coverage of the latter.

Spectral Mixture Models

Rover measurements $X = \{\mathbf{x}_1, \dots \mathbf{x}_n\}$ are spectra with tens or hundreds of wavelength channels; each spectrum is a vector $\mathbf{x} \in \mathbb{R}^d$. Roughly speaking, these *reflectance spectra* measure the fraction of light at each wavelength reflected from a surface. The spectral features reveal chemical and physical properties of the surface composition. A simple model for the reflectance of an extended object A is the integral of reflectances over its surface:

$$\mathbf{x}_A = \int_A \mathbf{x}_{dA} dA \tag{1}$$

This expression is valid as long as the observation geometry (observing angle, illumination angle and surface orientation) is approximately constant over A. It leads to a *geographic* or *areal* mixing model where each measurement is a mixture of a small number of *endmember* materials, the spectra of which combine in proportion to their physical extent on the surface (Keshava and Mustard 2002). Most scenes contain just a few endmember spectra; applying these in appropriate mixing fractions can reconstruct any measurement $\mathbf{x}$. For a scene with m endmembers the mixing fractions are vectors $\phi \in \mathbb{R}^m$. More generally we can model a spectral image using a library given by a $d \times m$ matrix Y, giving $\mathbf{x} = Y\phi$.

The elements of ϕ describe the library spectra fractional abundances within the geographic footprint of $\mathbf{x}$. This physical interpretation places certain restrictions on legal values of ϕ. Negative mixing fractions are impossible; one cannot, for example, observe a Mars surface pixel containing -5% Phyllosilicate clay. Thus ϕ is often constrained to be nonnegative. In addition, the fractional abundances should sum to unity, so many algorithms require $|\phi|_1 = 1$. These constraints force observations to be convex combinations of the endmembers, lying in the simplex bounded by elements Y.

There are several ways to determine the spectral library Y. Researchers have developed many automatic endmem-

ber detection algorithms that use statistics or convex geometry to estimate Y from data (Thompson et al. 2013). It is also common to build libraries from prior observations. For complete review of such algorithms we refer the interested reader to a comprehensive review by Plaza et al. (2009).

A typical unmixing problem starts with one or more observations $\mathbf{x}$ and a known endmember matrix Y. It seeks mixing fractions ϕ that accurately reconstruct the observations. It is typical to minimize the L2 norm of the error using Linear Least Squares (LLS), or Nonnegative Least Squares (NNLS) in the positive case (Lawson and Hanson 1974). The latter solves an optimization of the form:

$$\mathrm{argmin}_\phi \ \|Y\phi - \mathbf{x}\|_2 \text{ for } \phi \geq 0 \qquad (2)$$

Roughly speaking, one performs this operation at every pixel to map the areal abundance of each endmember material.

A least-squares solution gives nonzero mixing fractions for nearly all library spectra. This is physically implausible, since only a few materials would be present in one pixel. Thus, we will also consider a sparse mixing model. Multiple Endmember Spectral Mixture Analysis (MESMA) (Dennison and Roberts 2003) permits just a small fixed number of endmembers (typically two or three) to contribute to each remote spectrum. For each pixel one searches over all possible endmember combinations for each pixel, with mixing fractions computed using LLS or NNLS. The final model is the pair or triplet of endmembers having best reconstruction error for that pixel. MESMA models are common in disciplines from mineralogy to ecosystem studies (Roth, Dennison, and Roberts 2012; Fèvotte and Godsill 2006).

A successful unmixing provides a low reconstruction error, explaining and validating the remote observation. In addition, the list of endmembers is independently valuable since it identifies the purest spectral signals in the scene. It forms a compact spectral library capturing both common materials and any interesting outliers. Figure 1 shows an example from the Airborne Visible Near Infrared Imaging Spectrometer (AVIRIS) (Green et al. 1998). The scene shows an airborne image of a well-studied mining district in Cuprite, Nevada (Kruse 2002). We recognize distinct mineral classes from spectral absorption signatures at different wavelengths. Most other spectra in the scene are mixtures of these classes, so the endmember library is a powerful diagnostic and interpretive tool.

Approach

Formally, we aim to collect in situ measurements that best unmix the remote data. We define a set of candidate measurement sites $\mathcal{L}$. The robot collects *in situ* spectra by sampling at locations $B = \{b : b \in \mathcal{L}\}$. These multivariate measurements are written $\mathbf{y} = f(b) + \epsilon$. They are perturbed by Gaussian-distributed measurement noise ϵ. The entire set of future *in situ* measurements is $Y = \{\mathbf{y}_i : \mathbf{y}_i \in \mathbb{R}^d, 1 \leq i \leq m\}$. Together these observations form a spectral library, a random $m \times d$ matrix written Y_B. Good measurements reduce the total reconstruction error for remote sensing observations given by $X = \{\mathbf{x}_i : \mathbf{x}_i \in \mathbb{R}^d, 1 \leq i \leq n\}$. A resource cost $C(B)$ represents limited time, power and bandwidth; it must not exceed a total budget β. Without loss

of generality we assume the environment is planar and fully-navigable, so that the energy and time cost of traversal is proportional to the path length.

We define a risk function as the expected reconstruction error after unmixing the remote images with *in situ* spectra:

$$R(B) = E\left[\sum_{\mathbf{x} \in X} \min_\phi \|Y_B\phi - \mathbf{x}\|_2\right]$$
$$\text{for } \phi \geq 0, \ C(B) \leq \beta \qquad (3)$$

Note that the expectation is over the rover's observation matrix, which is a random variable. The expression is analytically challenging, so we solve the related minimization:

$$\mathrm{argmin}_B \ \sum_{\mathbf{x} \in X} \min_\phi \|E[Y_B]\phi - \mathbf{x}\|_2$$
$$\text{for } \phi \geq 0, \ C(B) \leq \beta \qquad (4)$$

The linear geographic mixing assumption (Equation 1) simplifies the expectation $E[Y_B]$ since reflectance spectra combine in proportion to their extent on the surface to make the remote pixel. As a consequence, the remote observation is the expectation of *in situ* measurements sampled uniformly at random from within their enclosing pixel. Writing X_B to signify remote measurements at sites B, we have:

$$R(B) = \sum_{\mathbf{x} \in X} \min_\phi \|X_B\phi - \mathbf{x}\|_2 \qquad (5)$$
$$\text{for } \phi \geq 0, \ C(B) \leq \beta \qquad (6)$$

One now can calculate the new objective explicitly for any candidate set of *in situ* measurements.

As the robot collects spectra, its observations reveal of some of the random variables in $E[Y]$. The matrix Z_A represents *in situ* spectra collected at previous locations $A = \{a : a \in \mathcal{L}\}$. These measurements are a realization of Y_A, and can be substituted into the expectation. After one or more observations, the library used for unmixing is the union of all measured spectra combined with the expected spectra to be collected at future locations. The objective is:

$$R(B|A) = \sum_{\mathbf{x} \in X} \min_\phi \| [Z_A \ X_B] \phi - \mathbf{x}\|_2$$
$$\text{for } \phi \geq 0, \ C(B) + C(A) \leq \beta \qquad (7)$$

Figure 2 illustrates the method. The rover is considering a path with two additional spectra Y_B. It composes a library of its collected spectra Z_A, together with the orbital data X_B used to estimate Y_B. It uses these signatures to unmix the spectra in the entire image. Further incorporating a MESMA sparsity constraint is straightforward; one simply requires that ϕ have mostly zero entries.

In general, a robot must pay a cost in time and power to move between locations. This is an *orienteering* problem where the total budget restricts path length, or alternatively, power and time resources required to complete the tour. We represent the plan as an ordered sequence of vertices $\mathcal{P} = [a_1, \ldots, a_m]$ which gives an ordering to the sample locations A. Algorithm 1 details a straightforward greedy procedure to optimize this objective subject to a path cost
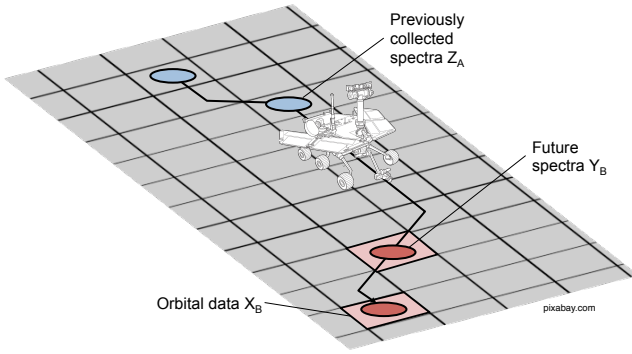
Figure 2: Spectra used in unmixing solution. The rover builds a library of collected spectra Z_A, combined with orbital data X_B that are used as proxies for future spectra Y_B.

budget $C(\mathcal{P})$. At each iteration we compute the best spectrum and then insert it into the sequence at the most desirable (cost minimizing) location. More sophisticated optimization strategies are possible, but the greedy approach is an effective and computationally-efficient approximation.

Input: Starting location v_{start},
  End location v_{end},
  Valid measurement locations Q,
  Associated remote measurements X,
  Total sample budget β
Output: Optimal plan $\mathcal{P}$

Initialize $A \leftarrow \{v_{\text{start}}, v_{end}\}$;
Initialize $\mathcal{P} \leftarrow [v_{\text{start}}, v_{end}]$;
while $C(\mathcal{P}) < \beta$ **do**
  for *each* $v \in Q \setminus A$ **do**
    form X_v by concatenation of X_A and x_v;
    compute
    $R(A \cup v) = \sum_{\mathbf{x} \in X} \min_\phi \|X_v\phi - \mathbf{x}\|_2$ for $\phi \geq 0$
    using NNLS;
    if $R(A \cup v) < R^\star$ **then**
      $R^\star \leftarrow R(A \cup v)$;
      $v^\star \leftarrow v$;
    end
  end
  Insert $v^\star$ into plan at the location minimizing $C(\mathcal{P})$
end

Algorithm 1: Greedy spectrum selection

Experiments

Datasets

We simulated an exploration scenario using high resolution airborne data as a proxy for *in situ* measurements. We used the Airborne Visible Near Infrared Spectrometer (AVIRIS) to simulate rover *in situ* spectra (Green et al. 1998). This instrument observes the spectral region from 0.38μm to 2.5μm at a spectral resolution of 0.01μm and high spatial resolution, making it comparable in spectral range and resolution to field instruments. Our case study centers on the mining

district of Cuprite, Nevada. It contains a wide range of distinctive mineralogical signatures, and has been extensively studied through scientific expeditions and field campaigns (Kruse 2002). The site exhibits mineralogical diversity with features at mutliple scales and wavelength regions. We used a sequence of three non-overlapping AVIRIS scenes from flight f970619t01p02r02, which we will call A, B, and C.

We also used orbital remote sensing data from the ASTER instrument (Fujisada 1995). This instrument's cameras have three VSWIR and six SWIR bands within this spectral range. In order to meaningfully compare the two instruments it is necessary to align them radiometrically and spatially. We began with ASTER Level 2 reflectance data with crosstalk correction (Iwasaki and Tonooka 2005), and used manually-selected ground control points to orthorectify the AVIRIS data to this coordinate frame via polynomial interpolation. We then transformed the ASTER reflectance values to match the AVIRIS atmospherically-corrected reflectance using a modified empirical line approach (Gao et al. 2009). We used AVIRIS pixels as ground truth and aligned the ASTER images to the corresponding reflectance values by fitting an independent gain to each channel.

Figure 3 shows scene C. The left panel shows the overlap area as a visible color (RGB) image. The right panel is a false color abundance map assigning each pixel to its dominant endmember. We generated it by using Vertex Component Analysis (Nascimento and Dias 2005) to identify endmember pixels. We then performed an unconstrained linear unmixing and classified pixels according to their largest constituent. This analysis was not used in the simulations but it helps to visualize the different spatial units.

Figure 4 has representative spectra from image locations I and II. They show both the AVIRIS spectrum and (corrected) ASTER data. ASTER has just a few channels; these can indicate the different units of surface material, but cannot conclusively determine the mineralogy. In contrast, the full-spectrum data by the AVIRIS instrument clearly resolves spectral features such as a shape indicative of Alunite (Spectrum I). The nine-band orbital product cannot conclusively identify these materials, but it is effective at localizing different surficial units to guide exploration.

Method

We simulated 256 random trials of hypothetical traverses. Each had a random start and finish location at the left and right of the image. We defined a path length budget of 125% of the Euclidean distance between start and end locations. This provided a challenging constraint with enough margin to visit a few targets of opportunity. We found that performance relationships generalized well to other path lengths. Each algorithm selected waypoints from a grid of candidate locations spaced at 20 pixels. The ASTER spectra associated with these grid points became our target library for the unmxing objective. We ran each trial using five different path planning options:

1. **Random path** selected each new waypoint at random, adding it to the waypoint sequence in the position that minimized path length.

2. **Direct path** selected each new waypoint in the order which minimized the total path length, and then exited when no further additions were feasible.

3. **Greedy Least Squares (LS)** applied algorithm 1 without positivity constraints on mixing fractions.

4. **Greedy Nonnegative Least Squares (NNLS)** applied algorithm 1, with positivity constraints.

5. **Greedy Multiple Endmember Spectral Mixture Analysis (MESMA)** used sparsity and positivity constraints.

The entire planning process took just a few seconds to run on a modern laptop computer.

In this first test we constructed the entire plan in advance so collected spectra did not influence the agent's path. However, in situ spectra could differ from expectations and an agent could account for this by revising its path after each acquisition. We evaluated this strategy with a second test that compared random, direct, and static Least Squares (LS) planners as well as an adaptive LS solution that replanned after every waypoint. We scored the paths for both tests by using the collected in situ spectra as a library to unmix the ASTER image with our most physically-plausible model (MESMA). The reconstruction error indicated whether the library of collected spectra was comprehensive. Relative performance of the different path planners was similar regardless of whether NNLS or MESMA were used during this final evaluation.
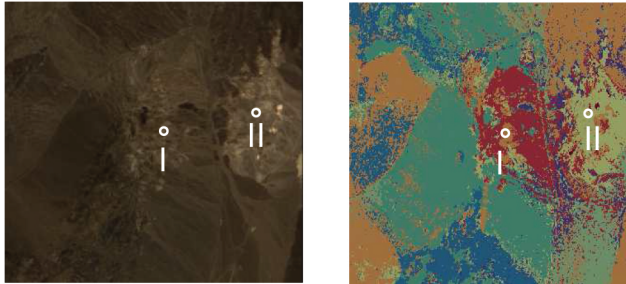

Figure 3: Original RGB image of Scene C, which is approximately 6 × 6 km, and false color image showing primary units. Spectra from locations I and II appear in Figure 4.

Results

Figure 5 shows a typical trial. The direct path, in black, traveled straight toward the goal while adding small wiggles to cover more terrain until exhausting the path length budget. The greedy planners moved in different directions to visit spectrally distinctive features. Figure 6 shows the performance scores over all runs, with boxes indicating data quartiles and median, and the whiskers indicating extrema. We noted several trends. First, the greedy adaptive approaches significantly outperformed the random and direct paths for all scenes ($p < 0.05$). For the most challenging scenes (A and C) the median unmixing per-pixel reconstruction error for the greedy NNLS algorithm was significantly better than the control cases. The Nonnegative Least
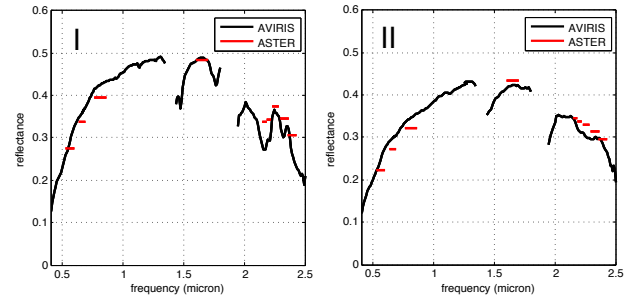

Figure 4: Spectra from locations I and II of Figure 3, showing low spectral resolution (ASTER) and high spectral resolution (AVIRIS) data.
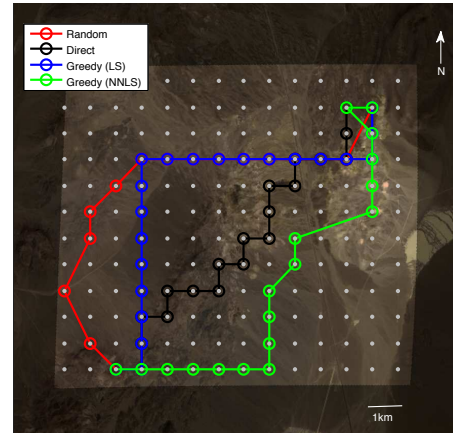

Figure 5: Example paths from the ASTER/AVIRIS simulation.

Squares approach slightly outperformed the unconstrained Least Squares method, but incorporating the MESMA constraint produced no further improvement. Figures 8 and 9 compare the error on a per-trial basis, showing NNLS against both a data-blind approach as well as unconstrained (LS) linear mixing. The best-fit line in red indicates that the spectrally-sensitive planning with a nonnegativity constraint improved performance at all three sites. Table 1 reports average scores, along with typical run times for unoptimized code running on a modern consumer-grade processor.

Figure 7 compares adaptive and non-adaptive algorithms.

	Direct	Random	Static LS	Adaptive LS
Site A	0.0201	0.0220	0.0144	**0.0131**
Site B	0.0105	0.0120	0.0096	**0.0088**
Site C	0.0194	0.0214	0.0133	**0.0122**

Table 1: Comparison of two science-blind planners and two science-aware planners. The table shows Root Mean Squared Error (RMSE) for 256 trials. The adaptive planner performed best, with significance to $p < 0.05$. It replanned after each waypoint to incorporate the latest science data.

	Direct	Random	LS	NNLS	MESMA
Site A	0.0194	0.0223	0.0142	**0.0132**	0.0138
Site B	0.0105	0.0121	0.0097	**0.0085**	0.0086
Site C	0.0193	0.0208	0.0136	**0.0125**	**0.0125**
Runtime	< 1 s	< 1 s	< 1 s	25 s	230 s

Table 2: Comparison of objective functions, similar to Table 1. LS: Least Squares. NNLS: Nonnegative Least Squares. MESMA: Multiple Endmember Spectral Mixture Model.
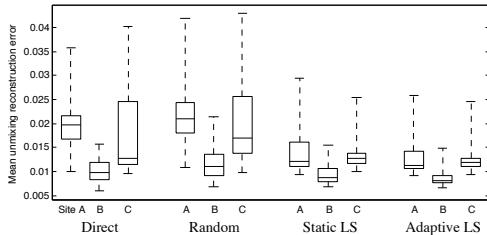
Figure 6: ASTER/AVIRIS simulation results comparing different replanning schedules.

The Adaptive method outperformed the static alternative, achieving the best overall reconstruction error of any method. During the trials we found that the collected data sometimes caused the rover to revise its original path. This represented recovery from missing signals that had not been found where expected, or bypassing future measurements made redundant by unexpected finds. The adaptive planner outperformed above the significance level, but the marginal benefit was small compared with the large difference from doing science-aware path planning in the first place. In some sense, this was encouraging - it suggested that the remote data is a good predictor of the *in situ* data. Adaptive replanning might also benefit the explorer by enabling graceful recovery from errors in plan execution, such as detours to avoid unforeseen navigation hazards.

Conclusion

This work presents an approach for autonomous robotic exploration that combines high-dimensional remote and in situ sensing at multiple spatial and spectral resolutions, while permitting strong correlations between measurement variables. We demonstrate that (1) for a given resource budget, explicit unmixing objectives result in more efficient exploration than *status quo* alternatives, (2) incorporating physically-motivated nonnegativity constraints can significantly help performance, and that (3) regular replanning provides limited additional benefit.

The method also applies to smaller environments. For instance, spectrometer panoramas, acquired at meter scales, could be selectively refined by targeted measurements of specific outcrops in the rover's local field of view (Wettergreen et al. 2014). Similar convex mixing assumptions would apply making the framework we have developed here applicable to a wide range of spectral exploration scenarios. Future work will validate the approach in the field using a rover-mounted VSWIR point spectrometer. Unlike the sim-
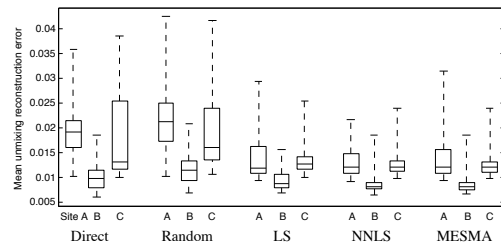

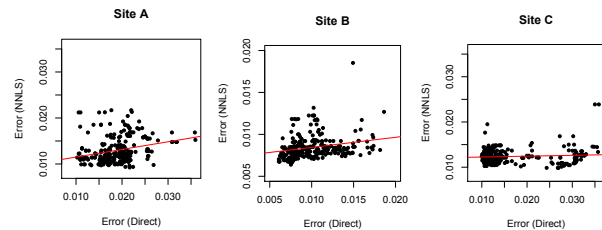Figure 7: ASTER/AVIRIS simulation results comparing different objective functions.

Figure 8: Comparison of per-trial error in reconstructed reflectance using planners that ignore spectral characteristics (Direct method, horizontal axis) and that incorporate nonnegative unmixing (NNLS, vertical axis)

ulations presented here, rover path planning in realistic environments will be dominated by concerns about navigability and hazard avoidance. The practical challenges of incorporating actual navigability into the path distance cost will be a primary concern as these techniques move from simulated environments into more realistic field settings.
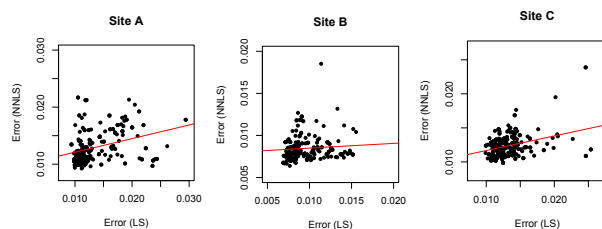
Acknowledgments

Figure 9: Comparison of per-trial error in reconstructed reflectance after planning based on unconstrained linear unmixing (LS, horizontal axis) and nonnegative unmixing (NNLS, vertical axis).

References

Bagnell, J. A.; Bradley, D.; Silver, D.; Sofman, B.; and Stentz, A. 2010. Learning for autonomous navigation. *Robotics & Automation Magazine, IEEE* 17(2):74–84.

Binney, J.; Krause, A.; and Sukhatme, G. S. 2010. Informative path planning for an autonomous underwater vehicle. In *Robotics and Automation (ICRA), 2010 IEEE International Conference on*, 4791–4796. IEEE.

Cao, N.; Low, K. H.; and Dolan, J. M. 2013. Multi-robot informative path planning for active sensing of environmental phenomena: A tale of two algorithms. *Proceedings of the 12th International Confer- ence on Autonomous Agents and Multiagent Systems (AAMAS)*.

Dennison, P. E., and Roberts, D. A. 2003. Endmember selection for multiple endmember spectral mixture analysis using endmember average RMSE. *Remote Sensing of Environment* 87:123–135.

Estlin, T.; Bornstein, B.; Gaines, D.; Anderson, R. C.; Thompson, D. R.; Burl, M.; Castano, R.; and Judd, M. 2006. AEGIS automated targeting for the MER opportunity rover. *ACM Transactions on Intelligent Systems Technology*.

Fèvotte, C., and Godsill, S. J. 2006. Bayesian approach for blind separation of sparse sources. *IEEE Trans. Signal Processing* 54(11):4133–4145.

Fujisada, H. 1995. Design and performance of ASTER instrument. In *Satellite Remote Sensing II*, 16–25. International Society for Optics and Photonics.

Gao, B.-C.; Montes, M. J.; Davis, C. O.; and Goetz, A. F. 2009. Atmospheric correction algorithms for hyperspectral remote sensing data of land and ocean. *Remote Sensing of Environment* 113:S17–S24.

Green, R. O.; Eastwood, M. L.; Sarture, C. M.; Chrien, T. G.; Aronsson, M.; Chippendale, B. J.; Faust, J. A.; Pavri, B. E.; Chovit, C. J.; Solis, M.; et al. 1998. Imaging spectroscopy and the airborne visible/infrared imaging spectrometer (AVIRIS). *Remote Sensing of Environment* 65(3):227–248.

Hollinger, G. A.; Pereira, A.; Ortenzi, V.; and Sukhatme, G. S. 2012. Towards improved prediction of ocean processes using statistical machine learning. *Proceedings of Robotics, Science and Systems*.

Iwasaki, A., and Tonooka, H. 2005. Validation of a crosstalk correction algorithm for aster/swir. *Geoscience and Remote Sensing, IEEE Transactions on* 43(12):2747–2751.

Keshava, N., and Mustard, J. F. 2002. Spectral unmixing. *Signal Processing Magazine, IEEE* 19(1):44–57.

Kruse, F. A. 2002. Comparison of AVIRIS and hyperion for hyperspectral mineral mapping. *JPL Airborne Geoscience Workshop, 11th, Pasadena (Califórnia), Proceedings, Jet Propulsion Laboratory Publication* 3–4.

Lawson, C. L., and Hanson, R. J. 1974. *Solving least squares problems*, volume 161. SIAM.

Low, K. H.; Dolan, J. M.; and Khosla, P. 2008. Adaptive multi-robot wide-area exploration and mapping. In *Proceedings of the 7th international joint conference on Autonomous agents and multiagent systems-Volume 1*, 23–30. International Foundation for Autonomous Agents and Multiagent Systems.

Nascimento, J. M. P., and Dias, J. M. B. 2005. Vertex component analysis: A fast algorithm to unmix hyperspectral data. *IEEE Transactions on Geoscience and Remote Sensing* 43(4).

Persson, M.; Duckett, T.; and Lilienthal, A. J. 2008. Fusion of aerial images and sensor data from a ground vehicle for improved semantic mapping. *Robotics and autonomous systems* 56(6):483–492.

Plaza, A.; Benediktsson, J. A.; Boardman, J. W.; Brazile, J.; Bruzzone, L.; Camps-Valls, G.; Chanussot, J.; Fauvel, M.; Gamba, P.; Gualtieri, A.; Marconcini, M.; Tilton, J. C.; and Trianni, G. 2009. Recent advances in techniques for hyperspectral image processing. *Remote Sensing of Environment* 113.

Roth, K. L.; Dennison, P. E.; and Roberts, D. A. 2012. Comparing endmember selection techniques for accurate mapping of plant species and land cover using imaging spectrometer data. *Remote Sensing of Environment* 127:139–152.

Silver, D.; Bagnell, J. A.; and Stentz, A. 2010. Learning from demonstration for autonomous navigation in complex unstructured terrain. *The International Journal of Robotics Research* 29(12):1565–1592.

Sofman, B.; Lin, E.; Bagnell, J. A.; Cole, J.; Vandapel, N.; and Stentz, A. 2006. Improving robot navigation through self-supervised online learning. *Journal of Field Robotics* 23(11-12):1059–1075.

Thompson, D.; Bornstein, B.; Chien, S.; Schaffer, S.; Tran, D.; Bue, B.; Castano, R.; Gleeson, D.; and Noell, A. 2013. Autonomous spectral discovery and mapping onboard the eo-1 spacecraft. *Geoscience and Remote Sensing, IEEE Transactions on* 51(6):3567–3579.

Thompson, D. R.; Wettergreen, D. S.; and Peralta, F. J. C. 2011. Autonomous science during large-scale robotic survey. *Journal of Field Robotics* 28(4):542–564.

Wagstaff, K.; Thompson, D. R.; Abbey, W.; Allwood, A.; Bekker, D. L.; Cabrol, N. A.; Fuchs, T.; and Ortega, K. 2013. Smart, texture-sensitive instrument classification for in situ rock and layer analysis. *Geophysical Research Letters* 40.

Wettergreen, D.; Wagner, M. D.; Jonak, D.; Baskaran, V.; Deans, M.; Heys, S.; Pane, D.; Smith, T.; Teza, J.; Thompson, D. R.; Tompkins, P.; and Williams, C. 2008. Long-distance autonomous survey and mapping in the robotic investigation of life in the atacama desert. In *International Symposium on Artificial Intelligence, Robotics and Automation in Space (iSAIRAS)*.

Wettergreen, D.; Foil, G.; Furlong, M.; and Thompson, D. R. 2014. Science autonomy for rover subsurface exploration of the atacama desert. *AI Magazine*.